AJNR

Helical CT Angiography: Dynamic Cerebrovascular Imaging in Children

Ronald A. Alberico, Patrick Barnes, Richard L. Robertson and Patricia E. Burrows

AJNR Am J Neuroradiol 1999, 20 (2) 328-334
http://www.ajnr.org/content/20/2/328

AJNR Am J Neuroradiol 20:328–334, February 1999

Helical CT Angiography: Dynamic Cerebrovascular Imaging in Children

Ronald A. Alberico, Patrick Barnes, Richard L. Robertson, and Patricia E. Burrows

BACKGROUND AND PURPOSE: **The purpose of this study was to assess the feasibility of helical CT cerebrovascular imaging (CTCVI) in children and to make initial comparisons with MR angiography and digital subtraction angiography (DSA).**

METHODS: **Twenty-six patients, ages 3 days to 17 years, were examined with CTCVI. Patients were scanned with 1-mm collimation and 2:1 pitch 30 seconds after the initiation of a hand injection of 2 mL/kg nonionic contrast material (320 mg/dL iodine) with a maximum dose that did not exceed 80 mL (minimum volume, 5 mL in a 2.5-kg infant). Reconstructions were done using maximum intensity projection and integral rendering algorithms. Four patients had CTCVI, MR angiography, and DSA (42 vessels studied) and nine patients had CTCVI and DSA (136 vessels studied). Scores of 1 (not present) to 3 (present in continuity to the first bifurcation) were assigned independently by two radiologists to 32 vessels in each correlated case for each available technique.**

RESULTS: **There were no technical failures. CTCVI depicted 18 thrombosed dural sinuses, three vascular malformations, one intracranial aneurysm, and four tumors. Ninety-five percent of the vessels seen with DSA were also seen with CTCVI. CTCVI identified all vessels seen on MR angiography.**

CONCLUSION: **Helical CTCVI is an effective technique for assessing the intracranial circulation in children. In this initial comparison, CTCVI showed more vascular detail than MR angiography, and had fewer technical limitations.**

The development of CT angiography proceeded from the combining of helical CT with advanced computer postprocessing algorithms (1–10). In particular, evaluation of the circle of Willis with CT angiography for the detection of aneurysms has achieved sensitivity and specificity approaching or exceeding the 90% level in several studies (3, 4). More recently, the intracranial venous circulation has been studied with CT to assess dural sinus thrombosis and to display the venous anatomy. CT venography is comparable to MR venography for the detection of dural sinus and deep cerebral venous thrombosis (11–13). CT angiography typically can be performed more rapidly than MR angiography and is less sensitive to motion artifacts. CT angiography has fewer problems related to patient compatibility than does MR angiography.

Received March 14, 1997; accepted after revision September 14, 1998.

From the Department of Radiology, Roswell Park Memorial Cancer Institute, Buffalo, NY (R.A.A.); and the Department of Radiology, Children's Hospital of Boston (P.B., R.L.R., P.E.B.).

Address reprint requests to Ronald A. Alberico, MD, 6296 Cloverleaf Circle, East Amherst, NY 14051.

Adult applications in CT cerebrovascular imaging (CTCVI) all require large volumes of contrast material (80–150 mL) and rapid injection rates (3–5 mL/s) via power injector. This approach is not feasible in most pediatric patients. To our knowledge, there have been no previous studies directly evaluating the use of helical CTCVI in children. Our purpose was to assess the feasibility of studying the intracranial circulation in pediatric patients using CTCVI, and to make initial comparisons of CTCVI with MR angiography and digital subtraction angiography (DSA).

Methods

Patients

Twenty-six patients between the ages of 3 days and 17 years (average age, 5 years) were studied with CTCVI. These included four patients less than 24 months old, two patients 3 to 4 years old, nine patients 5 to 10 years old, five patients 11 to 14 years old, and six patients 15 to 17 years old. Nine patients had DSA, six had MR angiography, and four had both MR angiography and DSA within the preceding 6 months. All patients except one were initially referred for contrast-enhanced head CT by clinical services. Patients who were selected for study with CTCVI had clinically suspected intracranial vascular disease, including dural sinus thrombosis, vascular malformation, and aneurysm. Other patients were scheduled for preoperative contrast-enhanced head CT for

frameless stereotactic planning, for radiotherapy planning, or as an adjunct to MR imaging. One patient was referred directly for CTCVI to further assess suspected sigmoid sinus thrombosis on a previous MR venogram.

Technique

CTCVI scans were obtained with helical technique using 1-mm collimation, 2:1 pitch, and 1-mm reconstruction intervals. The display field of view was 18 cm centered on the clivus, with a standard reconstruction algorithm. Scans were initiated 20 to 30 seconds after the start of a 2 mL/kg hand-injected bolus of nonionic contrast material (Optiray 320) via a peripheral intravenous site. The maximum volume injected was 80 mL. Iodine dose was 32 mg/kg with a maximum dose of 25 g. The injection rate was adjusted (when possible) so that two thirds of the dose was administered prior to the start of the scan. The remaining one third was injected continuously so that it was finished approximately 15 seconds before the completion of the scan.

Scan direction and prescan delay varied depending on the indication for the study. In patients with suspected venous disease or vascular malformations, scanning progressed in the cranial to caudal direction from the vertex of the skull to the skull base along a line parallel to the orbital roof for a distance of 12 cm (119 images). Injection delay was 30 seconds (23 patients). Scans for arterial detail (suspected aneurysms primarily) progressed in the caudal to cranial direction from the skull base to the vertex along a line parallel to the orbital roof. Injection delay was 20 seconds (three patients).

Radiation Dose

Radiation dose for the CTCVI examination was measured by using a standard CT dose index phantom with a 16-cm diameter and a 10.4-cm CT pencil ionization chamber. Dose measurements were made for CTCVI at 200 and 170 mA and 120 kV(p). Scan technique mimicked study parameters with a beam collimation of 1 mm and helical pitch of 2:1. Comparison measurements were made with our routine CT head protocols of continuous 5- or 7-mm sections with 200 or 170 mA and 120 kV(p). Scan volume was maintained constant for the comparison.

Postprocessing

All postprocessing was performed by a single radiologist using a 3D workstation (GE Advantage Windows 1.2, Milwaukee, WI). Data preservation techniques ensure that all available data from the initial scan are maintained in the volume of interest in the 3D model. This is achieved by avoiding the direct manipulation of data in the volume of interest during segmentation. Segmentation of the volume of interest is achieved by directly segmenting the unwanted areas of data and subtracting them from the main data set. We did this by using a technique of graded subtraction (13), in which unwanted pixels are initially separated from the main data set by density thresholding.

For CT, the high-density cortical bone of the skull is isolated first (the mask). Care is taken not to include vascular structures in the mask. This is achieved by setting a threshold that is above the upper limit of density for enhancing vessels in each patient. This can be done visually with the software provided. (In our study, the appropriate initial threshold varied depending on injection rate, patient size, hydration, and other factors, but was typically between 200 and 400 HU.) The dense bone is then subtracted from the main data set. What remains is all the original vascular and soft-tissue density and residual bone, which is similar in density to the vessels. The residual bone can be added to the high-density bone model (mask) through a process called dilation. Dilation adds a specified number of pixels around each existing pixel in a model in a density-independent manner. Alternating single-pixel dilation with subtraction allows complete removal of the skull, typically in two to four steps (about 10 minutes' work) without sacrificing vascular or soft-tissue detail. The skin is then removed in a similar manner.

The brain was completely segmented from the data set in all cases. Maximum intensity projection (MIP) images were produced and used in combination with superior and inferior cut planes in order to limit vascular overlap on the printed images. Integral rendering is a volume-rendering technique that preserves gray-scale information five voxels deep to the surface of a 3D model while providing a 3D perspective of the surface. This algorithm is a standard feature of the 3D workstation used and allows the display of structures that are just deep to the surface of a 3D model. The cortical veins are thus displayed with a 3D perspective without requiring their direct segmentation from the model.

DSA

DSA was performed in nine children under general anesthesia using the standard Seldinger technique. The number and extent of vessels studied were dictated by the patient's disorder. All cases were refilmed to include late-phase venous images to facilitate comparison with CTCVI. All DSA images were obtained within 6 months before CTCVI. The comparison was retrospective.

MR Imaging

MR angiography was performed with the 3D time-of-flight technique (flow compensation, magnetization transfer) at 47/3.1 (TR/TE). A superior saturation pulse was used to suppress venous signal. MR venography was obtained with the 2D phase-contrast technique and a velocity-encoding gradient of less than or equal to 10 mL/s.

Scoring and Statistics

CTCVI scans were divided into 32 individual vascular segments. Each vascular segment was scored by two neuroradiologists on a three-point scale (1 = not seen, 2 = seen discontinuously, 3 = seen continuously to the first bifurcation). The average number of cortical veins visible per case was calculated.

Weighted kappa correlation coefficients were estimated to assess agreement between the two readers for each of the three tests (Statxact 3 software, Cytel Software Corp, Cambridge, MA). Additional weight was given to vessels that were scored as absent (score = 1) by one reader and present (score = 2 or 3) by the other reader. Median scores for each vascular segment were calculated for all three techniques. The proportion of vessels that received a score of 2 or 3 on DSA (condition 1) and on MR angiography or CTCVI was calculated, along with the 95% confidence intervals for each reader. The proportion of vessels that received a score of 3 on DSA (condition 2) and on MR angiography or CTCVI was also calculated, along with the 95% confidence intervals.

Results

Twelve patients were examined for dural sinus thrombosis, 10 for preoperative planning, three for evaluation of an arteriovenous malformation (AVMs), and one for suspected subarachnoid hemorrhage. There were no technical failures.

Radiation dose for CTCVI as measured by a standard CT dose index phantom with a 10.4-cm pencil ionization chamber was 1.7 cGy for the 200-mA technique and 1.4 cGy for the 170-mA technique (1-mm collimation, 2:1 pitch, 12-cm volume). This

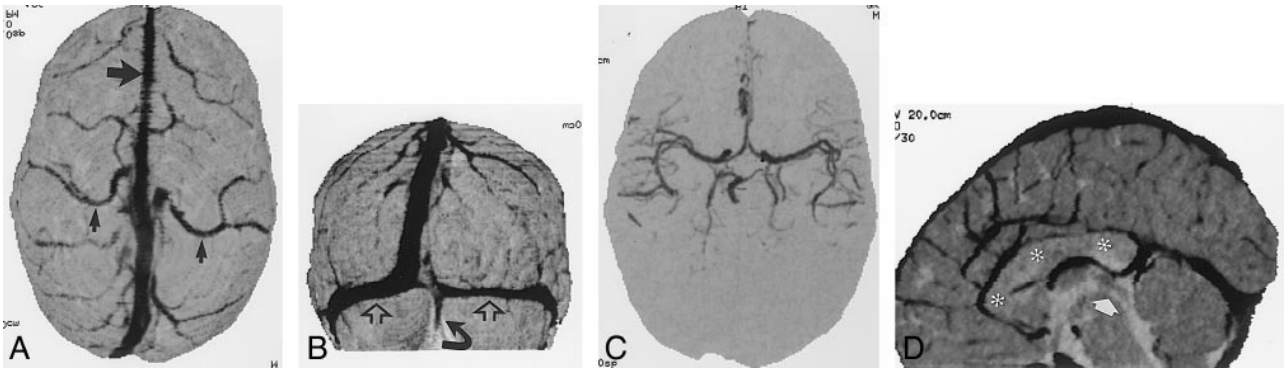

FIG 1. 4-year-old boy on L-asparaginase therapy.

A and *B,* Integral rendered CTCVI scans show detailed cortical venous anatomy, including the anastomotic veins of Trolard (*small closed arrows*), the superior sagittal sinus (*large straight arrow*), and the transverse (*open arrows*) and occipital (*curved arrow*) sinus.

C, The same data can be segmented to isolate the circle of Willis.

D, Integral rendering with sagittal cut planes reveals the patent sylvian aqueduct (*arrow*) and corpus callosum (*asterisk*), again from the same 60-second scan. Note the deep cerebral artery and venous detail.

FIG 2. 17-day-old boy who was clinically dehydrated with increased head circumference after resection of a medulloblastoma 2 days before these images were obtained.

A, Noncontrast vertex CT section shows high attenuation within the sagittal sinus and multiple cortical veins (*arrows*).

B, Integral rendered vertex view of a CTCVI scan clearly shows the lack of enhancement in the sagittal sinus and in several cortical veins (*arrows*). CTCVI confirms that the increased density on the noncontrast CT scan was related to thrombosis rather than to hemoconcentration.

C, Filling defect (*curved arrow*) in the transverse sinus is clearly seen in this posterolateral integral rendered image. Note the enlarged Labbé vein, which reconstitutes the sigmoid and jugular veins (*open arrow*).

D, Sagittal cut-plane reformatted image clearly shows the thrombosis of the superior sagittal sinus (*black arrow*), vein of Galen (*white arrow*), and torcular Herophili (*asterisk*).

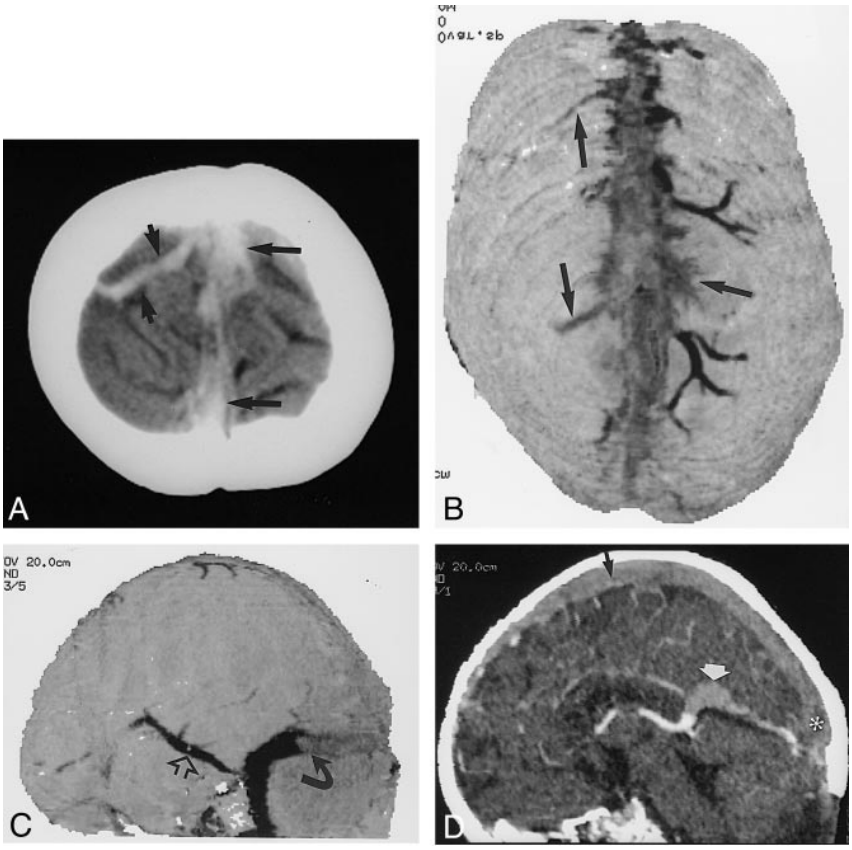

compares with our routine head CT dose of 4.5 cGy for the 7-mm collimation, 200-mA technique (14 sections).

CTCVI scans displayed with integral rendering revealed cortical vein detail without vascular overlap. Integral rendering in combination with sagittal cut planes allowed visualization of the cerebral aqueduct in 24 of 26 patients and of the corpus callosum in all 26 patients. MIP and cut-plane imaging allowed segmentation of the arterial anatomy from the venous anatomy in all 26 cases (Fig 1). Once segmented, the arterial anatomy could be subtracted from the venous anatomy for isolated display of the veins (26 of 26 cases). On average, postprocessing took 12 minutes by a radiologist experienced in image segmentation.

Eighteen thrombosed dural sinuses were diagnosed in five patients using previously established criteria for the CT diagnosis of dural sinus thrombosis, including visible intraluminal filling defects and the empty delta sign (13–17) (Fig 2). 3D models were used to help distinguish the empty delta sign from normal variations of the torcular Herophili.

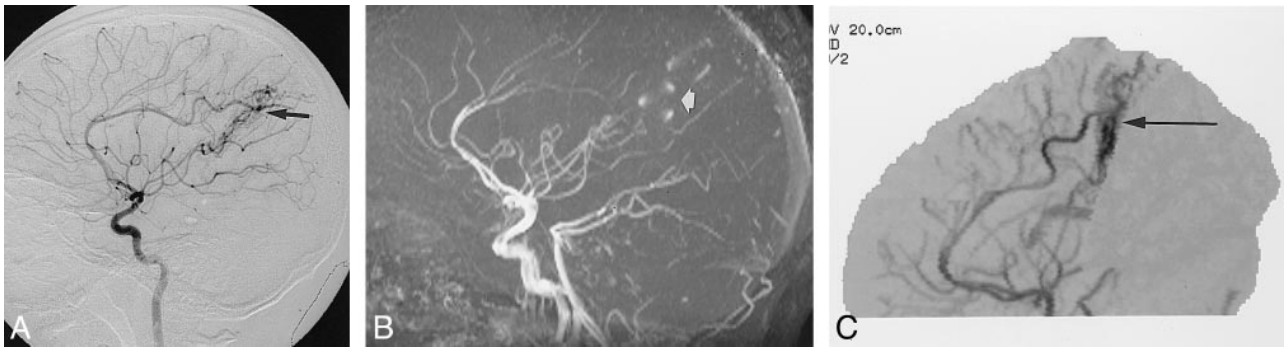

FIG 3. 9-year-old girl with a history of suspected AVM.

A, Lateral DSA image from a right internal carotid injection shows an AVM supplied by the pericallosal artery (*arrow*).

B, The AVM is seen less well on this lateral MIP image from a 3D time-of-flight MR angiogram (*arrow*), most likely owing to a combination of turbulence and in-plane flow artifacts.

C, The lateral MIP image of the CTCVI study is not susceptible to flow-related artifacts and clearly shows the malformation with its pericallosal supply (*arrow*).

Correlation with MR venography was available in two cases.

Vascular malformations and variations detected included three AVMs, one venous malformation with sinus pericranii, one cortical venous varix (surgically confirmed), and one fenestrated superior sagittal sinus (Fig 3). The average number of cortical veins identified per case was 4.6.

Table 1 lists the vascular segments scored and the number of data points available for each segment with each technique, along with the median score for each vascular segment. Comparison of the vascular scores for CTCVI and MR angiography/venography is provided in Table 2 for each reader for conditions 1 and 2 as defined in the Methods section. When vessels were considered visible on DSA (condition 1; score of 2 or 3), CT angiography agreed in 96% and 95% of cases for readers 1 and 2, respectively (95% confidence interval). When vessels were considered visible in continuity to the first bifurcation on DSA (condition 2; score of 3), CT angiography agreed in 88% and 88% of cases for readers 1 and 2, respectively (95% confidence interval). For the same comparison between DSA and available MR angiography, agreement was 77% and 81% for readers 1 and 2, respectively (condition 1), and 61% and 69% for readers 1 and 2, respectively (condition 2). Weighted kappa correlation coefficients for each test between the two readers were .66, .77, and .68 for CTCVI, MR angiography, and DSA, respectively (95% confidence). No significant difference in vascular detail was found among the different age groups studied with CTCVI.

Discussion

CT vascular imaging has been shown to have utility in the evaluation of intracranial arterial and venous anatomy in adults. Previous reports have shown efficacy in the evaluation of intracranial aneurysms (2–12) and have suggested that intracranial vascular malformations may also be studied with these techniques. Schwartz et al (11) retrospectively detected 87% of intracranial aneurysms (missing all aneurysms under 3 mm) while Schmid et al (12) reported 97.4% accuracy in detecting aneurysms. Casey et al (13) demonstrated that helical CT venography can display detailed cortical venous and deep cerebral venous anatomy with reproducible results, while Ozsvath et al (14) showed favorable comparison of CT venography with MR venography for the display of venous anatomy and the detection of dural sinus thrombosis. These studies were done primarily in adults, with injection rates and volumes that would exclude most pediatric patients (3 mL/s bolus with total volume from 80–150 mL).

The present study evaluated the feasibility of CT cerebrovascular imaging in pediatric patients using a hand-injected bolus of contrast material and a helical scanning technique. In radiographic examinations using intravenous contrast material in children, the injection rate, contrast volume, and radiation dose must be carefully considered. Our use of an increased helical pitch and relatively low milliampere current resulted in a radiation dose significantly lower than that incurred with our standard head CT technique. An additional benefit of increased pitch is decreased scan duration. Using this technique, the entire head can be scanned in 60 seconds. Shorter scan duration results in fewer motion artifacts. In this study, the lack of technical failures was in part due to the short scan duration. We limited the contrast dose to 2 mL/kg of nonionic contrast agent (320 mg/dL) with a maximum dose of 80 mL. A comparison between CTCVI contrast dose and the total contrast dose used in DSA is difficult because the DSA dose varies dramatically with indication. It is safe to say, however, that in small infants (3–10 kg), the CTCVI contrast volume was typically less than that used for routine cerebral angiography in this subgroup. With patients over 10 kg, CTCVI injection volume typically exceeded that used for angiography in uncomplicated cases. In no case was the volume of injection

TABLE 1: Median scores of vascular segments

Vascular Segment	CTCVI		MR Angiography/Venography		Digital Subtraction Angiography	
	No. of Vessels	(Median Score)*	No. of Vessels	(Median Score)*	No. of Vessels	(Median Score)*
Middle cerebral artery M1 right	17	(3)	8	(3)	11	(3)
Middle cerebral artery M1 left	17	(3)	8	(3)	10	(3)
Middle cerebral artery M2 right	17	(3)	8	(3)	10	(3)
Middle cerebral artery M2 left	17	(3)	8	(3)	10	(3)
Anterior cerebral artery A1 right	17	(3)	8	(3)	10	(3)
Anterior cerebral artery A1 left	17	(3)	8	(3)	10	(3)
Anterior cerebral artery A2 right	19	(3)	8	(3)	14	(3)
Anterior cerebral artery A2 left	19	(3)	8	(3)	12	(3)
Anterior communicating artery	17	(3)	8	(3)	10	(3)
Posterior communicating artery right	17	(2)	8	(2)	9	(3)
Posterior communicating artery left	17	(1)	8	(1)	10	(2.5)
Posterior cerebral artery right P1	17	(3)	8	(3)	10	(3)
Posterior cerebral artery left P1	17	(3)	8	(3)	10	(3)
Posterior cerebral artery right P2	17	(3)	8	(3)	10	(3)
Posterior cerebral artery left P2	18	(3)	8	(3)	10	(3)
Superior sagittal sinus	22	(3)	4	(2)	14	(3)
Inferior sagittal sinus	20	(3)	3	(1)	8	(2.5)
Transverse sinus right	21	(3)	4	(1.5)	13	(3)
Transverse sinus left	21	(3)	2	(2)	13	(3)
Occipital sinus	21	(3)	2	(1)	13	(1)
Labbé vein right	22	(2.5)	3	(1)	10	(2)
Labbé vein left	21	(2)	1	(1)	10	(2)
Trolard vein right	18	(3)	1	(2)	9	(1)
Trolard vein left	18	(2.5)	0	—	8	(3)
Straight sinus	22	(3)	0	—	11	(2)
Great vein of Galen	22	(3)	0	—	10	(2.5)
Internal cerebral vein right	22	(3)	0	—	10	(2.5)
Internal cerebral vein left	22	(3)	0	—	12	(3)
Rosenthal vein right	22	(3)	0	—	12	(3)
Rosenthal vein left	22	(3)	0	—	10	(2)
Thalamostriate vein right	22	(3)	0	—	12	(2.5)
Thalamostriate vein left	22	(3)	0	—	12	(2.5)

Note.—CTCVI indicates dynamic CT cerebrovascular imaging.
* Median score includes data from both readers.

TABLE 2: Comparison of CTCVI with MR angiography/venography and digital subtraction angiography

Technique	No. of Vascular Segments Compared	Reader 1: Percentage of Agreement with DSA*	Reader 2: Percentage of Agreement with DSA*
CTCVI condition 1 (score 2 or 3)	136	96	95
MRA/V condition 1 (score 2 or 3)	42	77	81
CTCVI condition 2 (score 3)	106	88	88
MRA/V condition 2 (score 3)	33	61	69

Note.—CTCVI indicates dynamic CT cerebrovascular imaging; MRA/V, MR angiography/venography; DSA, digital subtraction angiography.
* Agreement is calculated with 95% confidence intervals.

a limiting factor for the CTCVI examinations, and no patient was excluded from the study because of small size.

Our technique could be easily altered to emphasize venous anatomy by changing scan direction from caudal-cranial to cranial-caudal and by increasing the prescan delay from 20 seconds to 30 seconds. The vascular detail and average number of cortical veins per case identified in our pediatric population were similar to that previously reported by Casey et al (13) in adults. We found no significant difference in the characterization of vascular detail among the different age groups that we studied.

Our comparison of CTCVI with DSA for vascular identification uses DSA as the standard of reference. Although there were vessels identified on each CTCVI study that were not present on the DSA examinations, the DSA studies were frequently not optimized for visualization of the venous anatomy. In

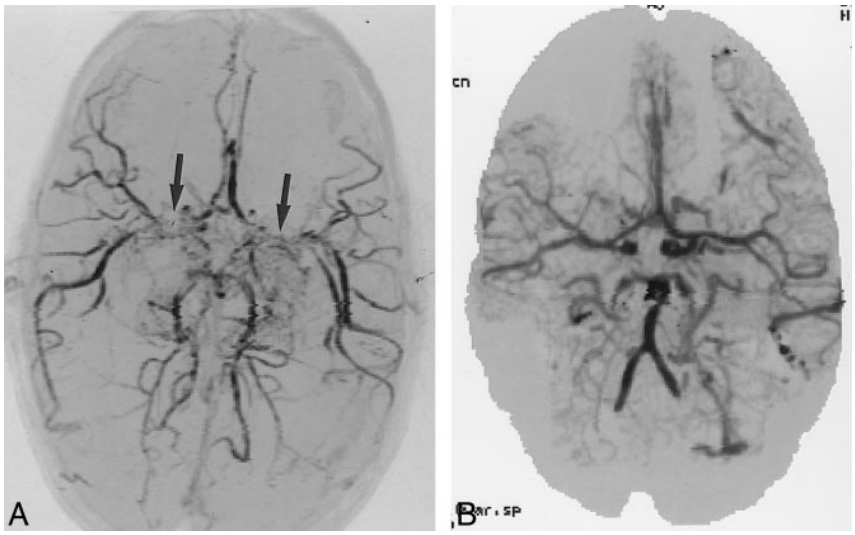

FIG 4. 4-year-old boy examined for increased head circumference and engorgement of superficial veins of the scalp.

A, 3D time-of-flight MR angiogram suggests moya-moya disease with bilateral supraclinoid carotid stenosis (*arrows*). The good flow distally in the middle cerebral arteries was puzzling.

B, CTCVI scan reveals patent proximal middle cerebral arteries as well as distal internal carotid arteries. Multiple small arteriovenous fistulas were also seen and confirmed at angiography. The MR signal loss was most likely related to the extremely high flow.

the 136 vessels available for correlation with DSA, CTCVI identified 96% and 95% for readers 1 and 2, respectively. The kappa values between readers were comparable for DSA and CTCVI (.66 and .68, respectively). The better correlation seen with MR angiography/venography ($\kappa = .77$) was most likely related to the smaller sample size. The most difficult vessels to identify were the posterior communicating arteries (Table 1), probably because of their relatively small size and low flow. In CTCVI, the proximity of these vessels to the skull base was also a likely contributory factor. Compared with DSA, CTCVI is relatively noninvasive, allows for virtually unlimited projectional views, and simultaneously displays adjacent parenchymal detail. Further prospective study is needed to determine the relative accuracy of CTCVI for detecting intracranial venous thrombosis and intracranial aneurysms in children.

In comparison with MR angiography/venography in our study, CTCVI was more invasive, involving the need for both iodinated contrast material and ionizing radiation. Advantages of CTCVI included fewer problems relating to patient compatibility and rapid scan time. The MR angiograms/venograms in our patients had more motion artifacts in general than the CTCVI scans. This was more likely due to the short duration of CTCVI than to any inherent insensitivity of the technique to patient motion. In addition, the short duration of CTCVI makes it more useful in the acute setting than MR angiography/venography. Patients with MR-incompatible life-support systems and biological implants can still be imaged with CTCVI. Although it was not analyzed in this study, we hypothesize that CTCVI in children may not require conscious sedation as frequently as MR angiography/venography does. Certainly, a formal study is required to confirm this hypothesis. Other artifacts, such as in-plane flow artifacts and turbulence-related signal loss, found on MR angiograms/venograms did not appear to affect the CTCVI scans (Fig 4). This may define a use of CTCVI as a problem-solving examination for ambiguous MR angiographic/venographic findings, eliminating the need for the more invasive DSA in some patients.

Our findings offer encouragement for the use of CTCVI in the evaluation of dural sinus and deep cerebral venous thrombosis. Before the development of MR venography, CT was the study of choice for evaluating dural sinus thrombosis. The use of intravenous contrast material in this setting became standard as a result of the realization that normal dural sinuses and deep cerebral veins can appear hyperdense, particularly in children (15, 17). Long scan times and thick-section collimation limited the efficacy of these early CT methods. In the adult population, it has been suggested that helical CT venography is an effective technique for assessing dural sinus and cerebral venous thrombosis (13–20). In the pediatric population, the study of choice for infants is Doppler sonography. Because of the limitations of MR venography related to in-plane flow artifacts and insensitivity to slow flow, CTCVI may prove to be a useful adjunct to this technique in older children. With patients who are acutely ill, or who have contraindications to MR imaging, CTCVI can serve as the primary technique for evaluating intracranial venous thrombosis.

The CTCVI technique can also be used to evaluate midsagittal anatomy in detail with multiplanar reformatted images and integral rendering (Fig 1). This technique was useful in depicting the extent of intracranial masses in pediatric patients while simultaneously delineating regional vascular detail. The inverted gray scale allowed improved visualization of vessels and gyral detail, with wider window settings than available with conventional display. Integral rendering preserved gray-scale information five voxels deep to the surface, which aided in visualizing intraluminal filling defects in the dural sinuses on the 3D models. Thick-section reformations of the data in the axial plane provided an acceptable alternative to routine

contrast-enhanced head CT in our preoperative planning patients, obviating additional postcontrast thick-section CT. The data generated were also compatible with radiotherapy and frameless stereotactic planning software.

The following limitations of CTCVI are noted: postprocessing of the data is required for 3D image production; although this took only 12 to 15 minutes in expert hands, there is a significant learning curve involved. 3D reconstruction is operator- and software-dependent. Reconstructions require a 3D workstation. Approximately 120 axial images are produced per case, which adds to expense in terms of data storage, even if source images are not printed on film. The CTCVI examinations required a hand injection with resultant radiation exposure to the radiologist. Finally, the relatively rapid scan time may not be sufficient for the enhancement of some types of disease processes.

Conclusion

CTCVI is a rapid, reproducible method of evaluating the intracranial circulation in children. It consistently identifies a high percentage of vessels visible on DSA. The technique is applicable to a wide range of pediatric patients with no statistical difference in vascular detail detected among the age groups. It has potential as an adjunct for preoperative planning and for the detection of intracranial venous thrombosis.

Acknowledgment

We thank William Greco, Department of Bio-mathematics, Roswell Park Memorial Cancer Institute, Core Grant Ca. 16056, for help with statistical analysis of the data.

References

1. Stehling MK, Lawrence JA, Weintraub JL, Raptopoulos XV. **CT angiography: expanded clinical applications.** *AJR Am J Roentgenol* 1994;163:947–955
2. Dorsch WC, Young N, Kingston RJ, Compton JS. **Early experience with spiral CT in the diagnosis of intracranial aneurysms.** *Neurosurgery* 1995;36:230–238
3. Vieco PT, Shuman WP, Alsoform GF, Gross CE. **Detection of circle of Willis aneurysms in patients with acute subarachnoid hemorrhage: a comparison of CT angiography and digital subtraction angiography.** *AJR Am J Roentgenol* 1995;165:425–430
4. Alberico RA, Patel M, Casey S, Jacobs B, Maguire W, Decker R. **Evaluation of the circle of Willis with three-dimensional CT angiography in patients with suspected intracranial aneurysms.** *AJNR Am J Neuroradiol* 1995;16:1571–1578
5. Hope JKA, Wilson JL, Thomson FJ. **Three-dimensional CT angiography in the detection and characterization of intracranial berry aneurysms.** *AJNR Am J Neuroradiol* 1996;17:439–445
6. Ogawa T, Okudera T, Noguchi K, et al. **Cerebral aneurysms: evaluation with three-dimensional CT angiography.** *AJNR Am J Neuroradiol* 1996;17:447–454
7. Liang EY, Chan M, Hsiang JHK, et al. **Detection and assessment of intracranial aneurysms: value of CT angiography with shaded surface display.** *AJR Am J Roentgenol* 1995;165:1497–1502
8. Zeman RK, Silverman MP, Vieco PT, Costello P. **CT angiography.** *AJR Am J Roentgenol* 1995;165:1079–1088
9. Wallace SK. **Current applications and techniques for computed tomographic angiography.** *Appl Radiol* 1996; Suppl:36–41.
10. Newell DW, Leroux PD, Dacey RG, Stimac GK, Winn HR. **CT infusion scanning for the detection of intracranial aneurysms.** *J Neurosurg* 1989;71:175–179
11. Schwartz RB, Tice HM, Hooten SM, Hsu L, Steig PE. **Evaluation of cerebral aneurysms with helical CT: correlation with conventional angiography and MR angiography.** *Radiology* 1994; 192:717–722
12. Schmid UD, Steiger HJ, Huber P. **Accuracy of high resolution computed tomography in direct diagnosis of cerebral aneurysms.** *Neuroradiology* 1987;29:152–159
13. Casey SO, Alberico RA, Patel M, Jimenez JM, Ozsvath RR. **Cerebral CT venography.** *Radiology* 1996;198:163–170
14. Ozsvath RR, Casey SO, Lustrin E, Alberico RA, Hassankhani A, Patel M. **Cerebral venography: comparison of CT and MR projection venography.** *AJNR Am J Neuroradiol* 1997;169: 1699–1707
15. Casey SO, Ozsvath RR, Alberico RA, Rubenstein D. **CT venography of dural sinus thrombosis.** *Radiol Soc North Am Elec J* 1998;2
16. Rao KCVG, Knipp HC, Wagner EJ. **Computed tomographic findings in cerebral sinus and venous thrombosis.** *Radiology* 1981;140:391–398
17. Segall HD, Ahmadi J, McComb JG, Zee C, Becker TS, Han JS. **Computed tomographic observations pertinent to intracranial venous thrombotic and occlusive disease in childhood.** *Radiology* 1982;143:441–449
18. Gabrielsen TO, Seeger JF, Knake JE, Stilwill EW. **Radiology of cerebral vein occlusion without dural sinus occlusion.** *Radiology* 1981;140:403–408
19. Goldberg AL, Rosenbaum AE, Wang H, Kim WS, Lewis VL, Hanley DF. **Computed tomography of dural sinus thrombosis.** *J Comput Assist Tomogr* 1986;10:16–20
20. Zilkha A, Stenzler SA, Lin JH. **Computed tomography of the normal and abnormal superior sagittal sinus.** *Clin Radiol* 1982; 33:415–425